Advances in Science and Technology Research Journal

Advances in Science and Technology Research Journal, 2026, 20(3), 350–364
https://doi.org/10.12913/22998624/213901
ISSN 2299-8624, License CC-BY 4.0

Received: 2025.10.07
Accepted: 2025.12.03
Published: 2026.02.01

Effectiveness of spin coating quantum dots deposition process onto mesoporous titanium dioxide for photovoltaic application

Paweł Kwaśnicki[1,2], Anna Gronba-Chyła[2], Agnieszka Generowicz[3*], Józef Ciuła[4], Zoia Duriagina[5], Viktor Koval[6], Tetiana Tepla[5], Piotr Herbut[7], Zbigniew Mucha[3], Dorota Mańkowska[8]

[1] Research & Development Centre for Photovoltaics, ML System S.A. Zaczernie 190G, 36-062 Zaczernie, Poland
[2] Faculty of Natural and Technical Sciences, The John Paul II Catholic University of Lublin, Konstantynów 1H, 20-708 Lublin, Poland
[3] Cracow University of Technology, Faculty of Environmental Engineering and Energy, Warszwska 24, 31-155 Cracow, Poland
[4] Institute of Engineering, State University of Applied Sciences in Nowy Sącz, ul. Zamenhofa 1A, 33-300 Nowy Sącz, Poland
[5] Department of Materials Science and Engineering, Lviv Polytechnic National University, 12 S. Bandera Street, 79013 Lviv, Ukraine
[6] Odessa Institute of Trade and Economics of Kyiv National University of Trade and Economics Odessa, Ukraine
[7] Department of Rural Building, Faculty of Environmental Engineering and Land Surveying, University of Agriculture in Cracow, 31-120 Cracow, Poland
[8] Institute of Natural Products and Cosmetics (I-52), Faculty of Biotechnology and Food Sciences, Lodz University of Technology, ul. Stefanowskiego 2/22, 90-537 Łódź, Poland
* Corresponding author's e-mail: agnieszka.generowicz@pk.edu.pl

ABSTRACT

The aim of this work was to present an effective method for deposition onto a conductive material covered by a thin film on a glass surface using the spin coating technique. The TiO_2 layer, consisting of 99% anatase particles (~20 nm diameter), was applied via screen printing to an estimated thickness of ~5 µm onto TCO-coated glass (NEC A7). QDs were deposited using spin coating with controlled parameters: time 90 s, rotational speed 4000 rpm, and acceleration A=100 rpm/s. Three types of colloidal QDs dispersed in toluene were utilized: ZnCuInS/ZnS (max. em 530 nm) ZnCuInS/ZnS and (max. em 700 nm), both at 1 g/ml concentration, applied in volumes of 250 µl and 500 µl; and CdS (max. em 460 nm) at 0.5 g/ml concentration, applied in volumes of 500 µl and 1000 µl. Selected samples underwent post-deposition annealing at 250 °C for 15 minutes. Surface morphology was characterized using Scanning Electron Microscopy (SEM) in the backscattered electron (BSE) detector configuration, while optical properties were assessed using double-beam spectrophotometer. In conclusion, the results confirm the effectiveness of the spin coating technique for QDs deposition onto TiO_2 layers, validating its potential to enhance optoelectronic performance through improved light absorption and charge separation dynamics crucial for QD-sensitized solar cell applications

Keywords: spin coating, transparent conductive oxide (TCO), quantum dots, photovoltaic.

INTRODUCTION

The increase in greenhouse gas emissions, ongoing environmental degradation, and excess waste [1], including the pollution generated by road transport make it necessary to move away from conventional energy sources. The transport based on fossil fuels significantly contributes to air pollution in urban areas and to the rise of global CO_2 emissions [2]. In response to these threats,

renewable energy sources (RES) are gaining importance as an ecological alternative supporting climate protection and public health.

The most important alternative energy sources include hydropower, biofuels, solar energy, wind energy, biomass, and geothermal energy [3, 4]. Increasing attention is also being paid to waste-derived fuels, which can be a significant energy source in distributed generation systems, such as ORC (Organic Rankine Cycle) systems, while also contributing to waste management and reducing pollutant emissions [5–7]. Each of these sources has its advantages and limitations; however, solar energy stands out as one of the most accessible, reliable, and economically viable solutions. The photovoltaic (PV) technology is widely recognized as a key component of the transition toward renewable energy systems due to its scalability, reliability, and relatively low maintenance requirements. In recent years, the use of renewable energy sources has significantly increased, supported by both technological advances and policy incentives. Among these, solar energy has attracted particular attention due to its global availability and steadily decreasing production costs [8–10].

A variety of solar cells have been developed, including crystalline silicon cells (c-Si), amorphous silicon cells (a-Si), dye-sensitized solar cells (DSSCs), hybrid solar cells [11–13], polycrystalline solar cells, monocrystalline solar cells (mono-Si), nanocrystalline solar cells, multijunction SCs, perovskite SCs, organic SCs, photoelectrochemical cells (PEC), plasmonic SCs, quantum dot SCs (QDSCs), multilayer SCs with a gradient band gap, and semiconductor SCs [14, 15]. A typical architecture of quantum dots solar cell consists of a substrate, usually glass, a conductive layer TCO and a photoanode layer, e.g. TiO_2. Transparent conductive oxides (TCOs) are the materials that exhibit both transparency and electrical conductivity, making them essential components in applications such as flat panel displays, solar cells, and electroluminescent devices, where they serve as transparent electrodes [16, 17]. The transparency of TCOs is characterized by high optical transmittance in the visible spectrum, which requires a bandgap exceeding 3.3 eV [18–20].

TCO layers are commonly employed as antireflective (AR) coatings in solar cells, often replacing silicon nitride. Among the wide array of materials available, indium oxide-based and zinc oxide-based compounds are the most prevalent choices. The optical and electrical properties of these layers play a critical role in the performance of solar cells and are intricately interrelated, meaning that they cannot be optimized independently. For instance, high carrier concentrations lead to a reduced refractive index of TCOs, even for the light with wavelengths significantly below 1100 nm, which compromises their AR performance [21, 22].

The key element of this photovoltaic device are quantum dots (QDs). Quantum dots are one of the most interesting objects in modern fundamental and applied solid state physics, including the applications for photovoltaics systems [23]. Colloidal QDs are semiconductor nanocrystals with radii smaller than the Bohr radius of the bulk material [24]. They exhibit discrete energy levels due to quantum confinement, which significantly alters interbank and intrabank relaxation processes [25]. Furthermore, colloidal QDs offer promising optoelectronic properties, including size-, shape-, and composition-dependent absorption edges, high absorption coefficients, large intrinsic dipole moments, and high photoluminescence quantum yields [26]. These extraordinary properties can be further enhanced by quantum mechanical effects, making QDs particularly advantageous for advanced optoelectronic applications [27].

In the context of photovoltaic devices, quantum dot solar cells capitalize on their unique ability to generate multiple excitons per photon, thereby reducing thermal losses and enabling higher electrical energy generation [28, 29]. Beyond functioning as independent functional layers in high-efficiency solar cells [30], QDs have also been utilized as additives to improve the quality of the active layer, enhance carrier transfer, and enable additional functionalities such as converting infrared or ultraviolet light into visible light, scattering and reflecting light, and absorbing heat [31, 32].

Incorporating QDs into perovskite films has shown to increase grain size, reduce recombination losses, improve charge extraction, enhance charge mobility, and broaden the spectral response range of the device [33]. These combined effects underscore the potential of QDs to revolutionize photovoltaic technology by enhancing efficiency and broadening application possibilities.

Typical sizes of the quantum dots of the order of 10 nanometers determine the majority of their physical properties, including the spectra of light

absorption and properties of light-injected carries [34, 35]. These spectra determine the application of quantum dots in photogalvanics and photovoltaic systems. In contrast to bulk materials, where free electron-hole pairs can be produced optically, a strong confinement of carriers in quantum dots and resulting interaction between them leads to formation of exciton-like states. This effect qualitatively modifies the optical properties of quantum dots and can make them useful for solar cell element applications [36, 37]. Semiconductor quantum dots are usually produced of two types of binary materials. The first type is usually referred to as III-V semiconductors, where one of the elements belongs to the III group [38, 39] of the periodic table of elements and the other belongs to the V group such as GaAs, InAs, InSb, and similar ones. The other group, named in the same way, is the II-VI semiconductors such as ZnS, ZnSe, CdS, and similar ones. In addition, coated quantum dots, where the core and the coating layer are made of different materials of the same (usually II-VI) type can be produced and used for different applications [40, 41]. Conventionally produced quantum dots show a variety of sizes and shapes. On one hand, this variety of quantum dot geometries extends the ability to use them for various applications, including photovoltaics [42].

Two-step thermal annealing significantly enhances the morphology of spin-coated films, enabling the development of highly efficient perovskite-based hybrid photovoltaic cells [43]. Functionalized spin-coated graphene films have been employed as transparent electrodes in polymer-fullerene photovoltaic devices (P3HT:PCBM). These graphene layers, with a thickness of 20 nm, exhibit a sheet resistance of 2 kΩ/sq and transparency exceeding 70% in the 400–1100 nm wavelength range [44].

When comparing spin-coated and blade-coated films, spin-coated films demonstrated a higher volumetric fraction of pure P3HT phases both before and after thermal annealing [45]. The application of silicon quantum dot (Si-QD) ink via spin-coating onto solar cell surfaces has been shown to enhance the performance of screen-printed silicon solar cells, attributed to increased light absorption facilitated by the porous Si-QD film [46]. Photovoltaic cells were fabricated using quantum dot-integrated polymer nanocomposites as an interfacial layer (electron extraction layer), consisting of carbon quantum dots dispersed via spin-coating onto ethoxylated polyethyleneimine [47].

Low-temperature-processed zinc oxide quantum dot-based thin films were developed using spin-coating deposition on flexible substrates, showcasing their potential for flexible photovoltaic applications [48]. Advances in colloidal quantum dot (CQD) inks have enabled the one-step spin-coating of compact CQD films with optimized thicknesses, achieving promising efficiencies in CQD-based photovoltaic cells (CQD-PV) [49]. Thin silicon dot (Si-dot) films, comprising Si dots dispersed in a ZnO:Bi matrix, were fabricated via spin-coating to optimize their optoelectronic properties. A high density of Si dots led to photoconductive quenching due to surface defect states, while low-density Si-dot films demonstrated a photoconductive gain of 10^3 times [50].

The versatility of spray-coating methods has also been explored in CQD solar cells, enabling fabrication on various previously unexamined substrate configurations. The potential for transitioning spray-coating techniques to roll-to-roll production was tested by applying CQD active layers onto six substrates mounted on a rapidly rotating drum, yielding devices with an average power conversion efficiency of 6.7% [51].

The aim of the analyses was to demonstrate an effective methodology for depositing colloidal quantum dots onto a layer covering a transparent conductive oxide (TCO) glass substrate using the spin coating technique, and subsequently to provide a comprehensive characterization of the resultant composite films regarding their surface morphology and optical properties.

The novelty of the proposed approach lies fundamentally in the demonstration and comprehensive verification of the effectiveness and controllability of the spin coating deposition process for colloidal QDs onto the specific architecture of the mesoporous TiO_2 photoanode, which is critical for third-generation photovoltaic applications. The use of spin coating allows for easy control over the thickness and quality of the QDs layer by adjusting process parameters such as time and rotational speed. Methodologically, the novelty is reinforced by the comparative application of three distinct colloidal QDs – two core/shell and one core material – with varying characteristic maximum emission wavelengths $l_{e\text{-}max}$460 nm, 530 nm and 700 nm, applied across a range of volumes 250 µl to 1000 µl.

Crucially, the study provides visual confirmation of the successful integration of these materials. Using Scanning electron microscopy

in the backscattered electron detector configuration, the research clearly demonstrated the presence of QDs as high-contrast bright spots on the TiO_2 matrix. This visual evidence confirms the effective anchoring of QDs TiO_2 matrix, thereby ensuring the required close interfacial contact. This intimate spatial arrangement is essential for maximizing light exposure, optimizing charge transfer kinetics, and minimizing the charge recombination losses between photogenerated electrons and holes.

MATERIALS AND METHODS

Sample preparation and quantum dot deposition

In this study, the process of depositing colloidal QDs onto a porous titanium dioxide (TiO_2) layer was presented. Although TiO_2 exhibits a relatively low quantum yield for solar energy photoconversion, it remains one of the most promising semiconductor materials for hybrid systems incorporating QDs due to its excellent chemical stability, suitable band alignment, and favorable charge transport properties.

The TiO_2 films were fabricated using Dyesol 18NR-T Transparent Titania Paste. This paste consists of approximately 99% anatase-phase TiO_2 nanoparticles with an average particle diameter of about 20 nm. The material exhibits a viscosity in the range of 40,000–55,000 mPa·s, ensuring its suitability for deposition by screen printing. Dyesol's 18NR-T paste is characterized by a high degree of nanoparticle dispersion and stability, optimized for use with a synthetic 43T mesh screen (KEY di Ennio, Pescara, Italy) to produce uniform, transparent photoanode layers.

From a materials perspective, TiO_2 serves as a chemically stable, wide-bandgap semiconductor ($E_g \approx 3.2$ eV) with excellent electron-transport properties and high surface area in its mesoporous form. However, its intrinsic limitation lies in poor visible-light absorption due to its wide bandgap. The incorporation of QDs – semiconducting nanocrystals with size-dependent optical properties – addresses this limitation by extending the absorption spectrum of TiO_2 into the visible and near-infrared regions. The conduction-band alignment between TiO_2 ($E_g \approx -4.0$ eV) and typical QDs, such as CdS ($E_g \approx -3.8$ eV) or ZnCuInS/ZnS ($E_g \approx -3.7$ eV), facilitates efficient electron injection from the photoexcited QDs into TiO_2, while TiO_2 simultaneously acts as an electron acceptor and transport medium, reducing recombination losses.

In this work, two types of core/shell quantum dots and one type of core-only colloidal quantum dots, each dispersed in toluene, were employed. QDs were selected based on their characteristic photoluminescence emission maxima at wavelengths of 460 nm, 530 nm, and 700 nm, respectively, corresponding to blue, green, and red spectral regions.

As substrates, Pilkington glasses coated with a transparent conductive oxide (TCO) layer (NEC A7, 2.2 mm thickness, optical transmittance Lt = 82%) were utilized. Prior to TiO_2 coating and QD deposition, the glass substrates were degreased and cleaned following a standardized cleaning protocol to remove organic and particulate contaminants.

ZnCuInS/ZnS quantum dots were chosen as low-toxicity, environmentally benign alternatives to conventional Cd- or Pb-based QDs. Their tunable bandgap energy (1.6–2.4 eV) enables broad absorption spanning the visible to near-infrared region, making them ideal for enhancing solar photon utilization. The zinc sulfide (ZnS) shell serves as a passivating barrier that effectively suppresses surface trap states, improving photoluminescence quantum yield and long-term photochemical stability. Moreover, the favorable conduction band alignment between ZnCuInS ($E_{CB} \approx -3.7$ eV) and TiO_2 ($E_{CB} \approx -4.0$ eV) allows efficient photoinduced electron injection, while maintaining chemical compatibility with oxide surfaces. This combination makes ZnCuInS/ZnS QDs particularly suitable for exploring charge-transfer dynamics and light-harvesting efficiency in eco-friendly hybrid photoanodes.

In contrast, CdS quantum dots were selected as a reference system due to their well-documented electronic structure, narrow size distribution, and strong absorption edge in the blue region (≈460 nm, Eg ≈ 2.7 eV). CdS exhibits excellent charge carrier mobility and rapid electron injection kinetics into TiO_2, as extensively reported in QD-sensitized solar cells and photocatalytic studies. By comparing CdS-based hybrids with ZnCuInS/ZnS systems, it becomes possible to distinguish the influence of core composition and surface passivation on optical response, interfacial charge transfer, and photostability.

Thus, the combined use of CdS (benchmark, high-injection efficiency) and ZnCuInS/ZnS (low-toxicity, broad-spectrum) nanocrystals provides a comprehensive framework for evaluating the structure–property relationships in QD/TiO_2 interfaces, bridging performance and sustainability considerations in next-generation optoelectronic materials.

For the deposition process, a spin coater system (model WS-650Mz-23NPPB, Laurell Technologies Corporation) was employed. The coater is equipped with a 241 mm chamber and a vacuum holder fitted with a 45 mm polypropylene adapter, ensuring secure fixation and uniform rotation of the substrates. Before the deposition of QDs, all TiO_2-coated substrates were rinsed with high-purity isopropyl alcohol to eliminate residual impurities and subsequently dried using a stream of high-purity compressed air. This preparation ensured optimal surface cleanliness and adhesion of the colloidal QDs to the TiO_2 layer.

The spin-coating method was selected for QD deposition due to its distinct advantages in producing uniform, reproducible thin films with precise control over thickness and surface coverage. During spin coating, centrifugal forces distribute the QD colloidal suspension evenly across the TiO_2 surface, while solvent evaporation ensures the formation of a dense, homogeneous nanocrystal layer. Compared to alternative deposition techniques, such as dip-coating, electrophoretic deposition, or drop-casting, spin coating offers superior film uniformity, minimal agglomeration, and compatibility with low-temperature processing – the features that are particularly important for maintaining QD optical integrity and preventing degradation of core/shell structures.

Furthermore, spin coating allows fine-tuning of the QD surface concentration by adjusting operational parameters, such as solution viscosity, spin speed, and acceleration rate. This control enables systematic modulation of the optical density and interference patterns observed in UV–VIS–NIR spectra, providing direct feedback on film thickness and morphology. The method also preserves the colloidal nature and ligand coverage of QDs, which are essential for ensuring adequate adhesion to the TiO_2 substrate and maintaining photostability under illumination.

From a functional standpoint, the use of spin-coated QDs on TiO_2 enhances the light-harvesting efficiency through spectral broadening and enables interfacial charge transfer processes analogous to those in dye-sensitized or perovskite-based solar architectures. The hybrid system combines the high optical tunability of QDs with the efficient electron transport of TiO_2, making it an attractive platform for applications in quantum dot–sensitized solar cells, photocatalytic hydrogen generation, and photodetector devices.

The interface between the colloidal QDs and the TiO_2 matrix plays a critical role in determining the overall photoelectronic performance of the hybrid system. Upon illumination, photogenerated electrons in the conduction band of the QDs can be injected into the TiO_2 conduction band, facilitating charge separation and reducing recombination losses. The efficiency of this process strongly depends on the energy alignment between the QD conduction band minimum and the TiO_2 conduction band edge, as well as on the surface chemistry and the presence of passivating ligands.

In the case of core/shell QDs, the shell material serves as a passivation layer that minimizes the nonradiative surface trap states while maintaining favorable electronic coupling with TiO_2. The surface ligands surrounding the QDs – often long-chain organic molecules – can inhibit charge transfer; therefore, partial ligand exchange or surface modification is typically employed to enhance thr electronic communication between QDs and TiO_2. Additionally, strong electrostatic or covalent interactions between the QDs and surface hydroxyl groups of TiO_2 can promote effective anchoring as well as improve electron transfer kinetics across the interface.

The overall photocurrent generation efficiency of such QD/TiO_2 assemblies thus arises from a delicate balance between surface passivation, energy level alignment, and charge transfer dynamics. Optimizing these parameters is essential for the development of high-performance quantum dot–sensitized or hybrid photovoltaic devices.

Experimental procedures

For comprehensive characterization of the examined quantum dot–TiO_2 composite samples, two complementary analytical techniques were employed: Scanning electron microscopy (SEM) and UV–VIS–NIR spectroscopy. Each technique provided distinct, yet interrelated insights into the morphological and optical properties of the investigated materials.

SEM was utilized to assess the surface morphology, homogeneity, and structural integrity of the TiO_2 layer following QD deposition. High-resolution imaging and nanoscale surface characterization were performed using a dual-beam FEI Quanta 3D FEG system (Hillsboro. Oregon USA). This instrument is equipped with a versatile suite of analytical and manipulative modules, enabling the application of multiple imaging and microanalytical techniques within a single vacuum chamber.

SEM was operated in both low-vacuum backscattered electron (BSE) and secondary electron (SE) modes to evaluate surface topology, pore distribution, and QD coverage uniformity. Additionally, ion-induced secondary electron (ISE) imaging was employed for enhanced contrast of nanostructured features, while energy-dispersive X-ray spectroscopy (EDS) was used for qualitative and semi-quantitative elemental composition analysis, confirming the presence and spatial distribution of Ti, O, and QD-related elements (e.g., Cd, Se, or Pb). The accelerating voltage was varied between 1 and 2 keV, and the working distance was adjusted within 2–4 mm, depending on the surface topography and the required spatial resolution. The system allowed for magnifications up to 300,000×, enabling precise visualization of nanoscale structural features, such as QD aggregates and surface roughness variations within the mesoporous TiO_2 network.

UV–VIS–NIR spectroscopy (Jasco V-670, Hachiōji, Tokyo, Japan) was employed to investigate the optical absorption characteristics and to confirm the photoactivity of the deposited QDs. Measurements were conducted at room temperature using a double-beam spectrophotometer, which ensures high stability and accuracy by simultaneously recording sample as well as reference spectra. The spectrophotometer was equipped with a deuterium lamp (emission range 190–350 nm) and a halogen lamp (emission range 330–2700 nm) as light sources, enabling comprehensive spectral coverage across the ultraviolet, visible, and near-infrared regions.

Detection was performed using a PbS photomultiplier, offering high sensitivity in the NIR region. The photometric accuracy of the system was ±0.002 ABS for absorbance values between 0–0.5 ABS, ±0.003 ABS for the 0.5–1.0 ABS range, and ±0.3%T for transmittance measurements. This configuration allowed the acquisition of precise absorption spectra, from which optical band gaps and quantum confinement effects in the QDs could be evaluated. The obtained spectral data confirmed the presence of size-dependent excitonic absorption features and validated the successful optical activation of the QD layer following deposition onto the TiO_2 substrate.

The combined SEM and UV–VIS–NIR data provided a comprehensive understanding of the relationship between the morphological characteristics and the optical response of the QD/TiO_2 hybrid layers. SEM micrographs revealed that QDs were uniformly distributed across the porous TiO_2 surface, forming a continuous and homogeneous coverage without significant agglomeration. The observed pore structure ensured sufficient surface area for QD anchoring and effective electronic coupling between the QD layer and the TiO_2 scaffold.

Correlating these morphological findings with the optical absorption data demonstrated that the samples with more uniform QD coverage exhibited enhanced and broadened absorption in the visible spectral range, confirming efficient photon capture and the expected quantum confinement effects. The presence of distinct excitonic peaks in the UV–VIS–NIR spectra further validated the preservation of the QD optical properties after deposition, while the absence of significant spectral shifts indicated minimal QD aggregation or degradation during processing.

Together, these analyses confirmed that the deposition method preserved the structural and optical integrity of the quantum dots while ensuring their efficient integration into the TiO_2 matrix – an essential condition for achieving effective photoinduced charge transfer and improved performance in hybrid photovoltaic or photocatalytic systems.

RESULTS

A layer of TiO_2 paste (18NR – T Dyesol) was applied to the prepared glass. Substrate for the TiO_2 deposition was glass coated with FTO thin layer with a thickness of around 600 nm, which is a widely used architecture for the building of a DSSC or QDs solar cell. TiO_2 layer was made using screen printing technology and the thickness of the layer was estimated to be in the range of 5 µm, according to the deposition process. The prepared samples were heated in a furnace according

to a given temperature profile and then subjected to the fusing process, as listed in Table 1.

A layer of quantum dots was applied on prepared substrates using the spin coating method. Deposition process parameters: Time – 90 s, Rotational speed – 4000 rpm, acceleration A=100 rpm/s. Quantum dots with various geometric and opto-electronic parameters were used for the studies. Due to the easy separation of exciton for the photovoltaic application the focus was mainly on quantum dots of the second type. Table 2 presents selected quantum dots and their parameters:

After applying quantum dots to the substrates, half of the samples were annealed at 250°C for 15 minutes.

The surface investigations were performed using high-resolution scanning electron (SEM). SEM FEI = for sample imaging was used. SEM was equipped with in-column backscatter detector (ICD) which provides no loss material contrast, mirror detector (MD) which provides low loss material contrast, ICD detector enabling low kV resolution at high immersion ratios and energy dispersive spectroscopy (EDS) detectors. The images were registered at the accelerating voltage varied from 1 to 2 keV and working distance between 2 and 4 mm.

A typical image of the photoanode topography is shown in Figure 1.

Figure 2 shows the surface of the TiO_2 substrate with visible low-dimensional structures. When comparing the contrast of Figures 1 and 2, a significant difference can be seen, which results from the detector used. Figure 1 shows the surface topography in the best possible topographic contrast, in the second case the distinction in mass contrast was important, hence the surface is much less separated. Nevertheless, interesting information was obtained, visible bright spots were identified as objects with a much higher atomic mass than the substrate. This clearly indicates the presence of quantum dots, which as objects consisting of heavier elements (higher Z number) are visible as bright spots against the background of an almost homogeneous substrate. QDs are visible both in TiO_2 crystallites and in the gaps between the meso porous structure of the substrate. Quantum dots should be deposited directly onto the surface of the mesoporous TiO_2 layer to ensure intimate contact between the QDs and the semiconductor matrix. Since QDs serve as sensitizers that absorb incident light and generate excitons (electron-hole pairs), placing them on the surface of TiO_2 crystals maximizes the exposure to light and enables tuning of the absorption spectrum through quantum size effects. The photoexcited electrons from the QDs are injected into the conduction band of TiO_2. For this to occur efficiently, QDs must be in close electronic contact with the TiO_2 surface to minimize interfacial resistance and enhance charge transfer kinetics. Additionally by anchoring QDs directly onto TiO_2 crystals and covering the surface uniformly, the likelihood of charge recombination between photogenerated electrons and holes is reduced. While the majority of QDs should be on the outer surface of the mesoporous TiO_2 structure, some penetration into the porous structure is beneficial for enhancing light harvesting through multiple scattering and increased surface area.

Before spectroscopic studies, the samples were cleaned. The background air was removed from the spectra. Then, measurements of the optical properties of glass, glass with a TiO_2 coating and coatings with quantum dots were performed. The samples that had been annealed beforehand were used for the studies. Exemplary results are presented in Figure 3.

A clear signature of presence of QDs layer is visible comparing spectrum of TCO or TCO/TiO_2 samples. An increase in transmittance in the IR

Table 1. Temperature profile parameters of heating and fusing processes

Heating temperature profile	Temperature profile of the fusing process
1 h →480 °C 1 min w 480 °C 4 min →530 °C 15 min w →530 °C 7 min→550 °C	55 min →520 °C 5 min w 520 °C 10 min →670 °C 5 min w →670 °C

Table 2. Summary of QDS parameters used for the deposition process

Nr	Quantum dots	Quantum dot concentration in toluene	Volume of applied material	
1	ZnCuInS/ZnS (max. em 530 nm)	1 g/1 ml	250 µl	500 µl
2	ZnCuInS/ZnS (max. em 700 nm)	1 g/1 ml	250 µl	500 µl
3	CdS (max. em 460 nm)	0.5 g/1 ml	500 µl	1000 µl

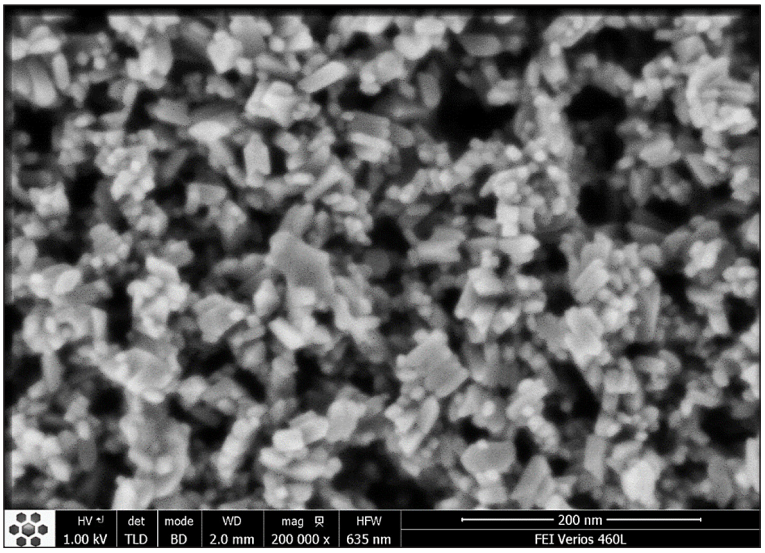

Figure 1. SEM image for the mesoporous TiO_2 substrate

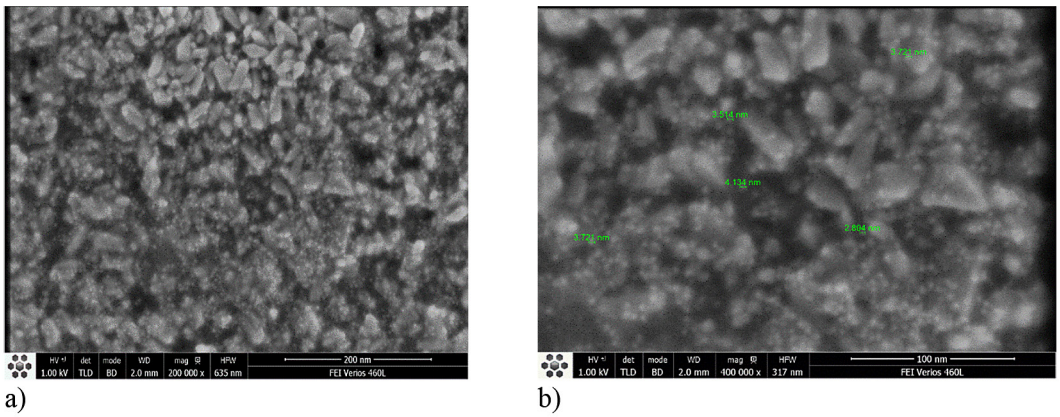

a) b)

Figure 2. SEM images for a mesoporous TiO_2 substrate with deposited quantum dots in the: a) secondary, b) backscattered electron detector configuration

region is noticeable. Additionally for the samples with thin TiO_2 layer and with QDs characteristic fringes related to interference pattern from thin film are visible. Lack of fringes for higher QDs concentration (500 µl) may be related to a much thicker layer formed after the deposition process. For the samples with QDs characterized by wavelength of maximum emission $l_{e\text{-}max}$ = 700 nm (Figure 4) a significant decrease in transmittance in VIS region is observed. This is due to broad absorption line corresponding to this QDs.

Since the bandgap energy of quantum dots (QDs) is inversely proportional to their particle size, the QDs with an emission maximum at 700 nm possess larger diameters than those emitting at 530 nm. Consequently, during the spin-coating process, the smaller QDs ($l_{e\text{-}max}$ = 530 nm) are more susceptible to outward displacement under the influence of centrifugal forces, leading to a reduced surface concentration and a thinner deposited layer. In contrast, the larger QDs $l_{e\text{-}max}$ = 700 nm) experience a lower degree of radial migration and remain more uniformly distributed across the substrate, resulting in a denser and optically thicker film. This size-dependent behavior directly contributes to the observed differences in optical absorption intensity and interference fringe contrast, confirming the strong correlation between QD dimensions, centrifugal dynamics, and film morphology in the spin-coating process.

Figure 5 presents a comparison of transmittance changes as a function of wavelength for a TiO_2 substrate with deposited CdS quantum dots exhibiting an emission wavelength of 460 nm. The orange line represents TCO glass, while the blue line corresponds to TCO glass coated with a

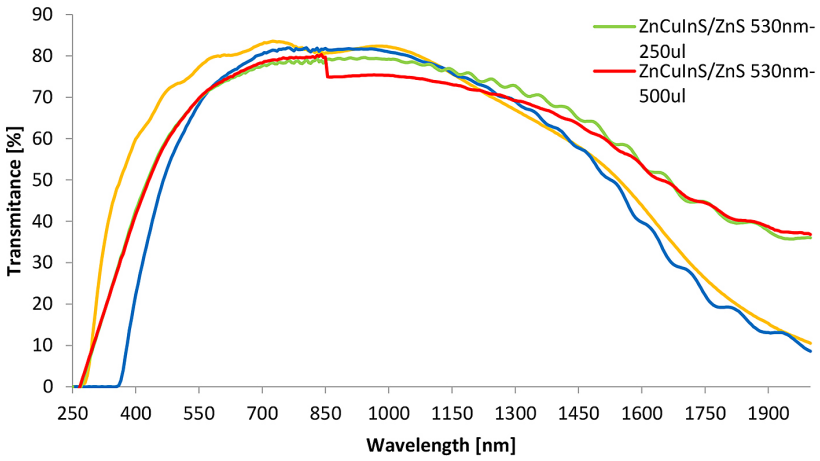

Figure 3. Comparison of transmittance changes as a function of wavelength for the TiO_2 substrate with ZnCuInS/ZnS 530 nm quantum dots deposited (orange line TCO glass, blue TCO glass with TiO_2)

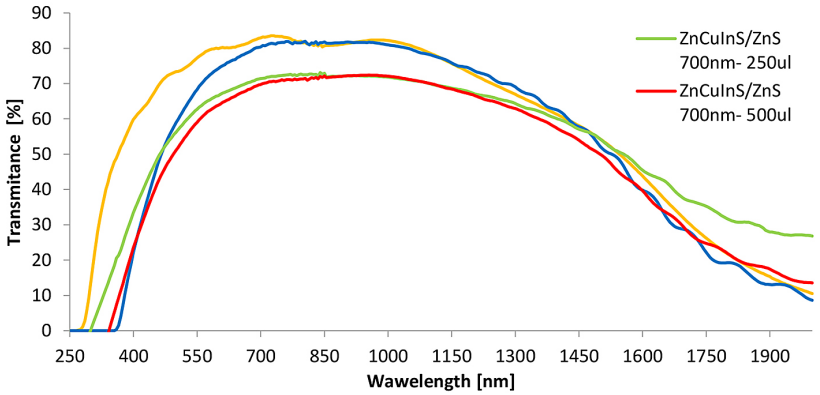

Figure 4. Comparison of transmittance changes as a function of wavelength for the TiO_2 substrate with ZnCuInS/ZnS 700 nm quantum dots deposited (orange line TCO glass, blue TCO glass with TiO_2)

TiO_2 layer. The analysis of these spectra allows for observation of the influence of both the thin TiO_2 coating and the presence of quantum dots on the optical properties of the sample, particularly in the visible range, where changes in transmittance may be related to absorption characteristic of the applied CdS quantum dots.

DISCUSSION

The optical and morphological characterization of the QD/TiO_2 hybrid structures demonstrates close agreement with the established models of semiconductor nanocomposites, confirming the reproducibility of the employed deposition process and the effective integration of QDs within the porous TiO_2 matrix. The UV–VIS–NIR spectra revealed distinct excitonic absorption peaks corresponding to the QDs with emission maxima at 460 nm, 530 nm, and 700 nm. The measured absorption edges were located at approximately 2.70 eV, 2.35 eV, and 1.75 eV, respectively, which are in excellent agreement with the size-dependent bandgap energies predicted by quantum confinement theory for CdS- and Zn–Cu–In–S–based QDs. A red shift of ≈30–40 nm was observed as the QD size increased, consistent with the trend reported by Kamat et al. [52], who observed a similar spectral displacement (≈25–45 nm) in the CdSe–TiO_2 assemblies due to relaxation of confinement. In the present study, the samples containing red-emitting QDs (λ_em = 700 nm) exhibited enhanced absorption in the visible and near-infrared regions (600–900 nm), with an optical density increase of up to 25% compared to green-emitting QD samples. This increase can be attributed to higher QD loading and stronger interband absorption. Comparable enhancement levels (20–30%) have been

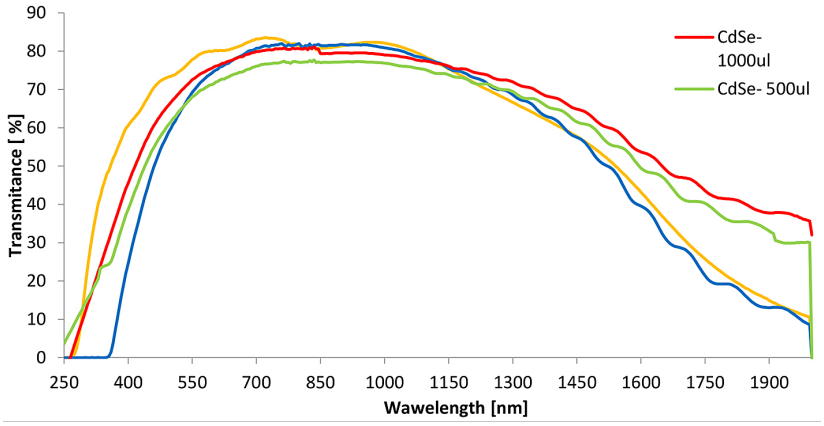

Figure 5. Comparison of transmittance changes as a function of wavelength for the TiO_2 substrate with 460 nm CdS quantum dots deposited (orange line TCO glass, blue TCO glass with TiO_2)

reported by Jin et al. [53] for Zn–Cu–In–S/ZnS QDs deposited on TiO_2 films, supporting the notion that controlled QD loading improves visible light utilization without introducing detrimental optical scattering. Conversely, the green-emitting QDs (λ_em = 530 nm) produced minimal alteration in transmittance within the visible range, indicating limited surface coverage and lower optical path-length modulation. This observation is consistent with the findings of Kumar et al. [54], who reported that thin CdSe/ZnS coatings yielded negligible absorption enhancement when the QD layer thickness remained below 80 nm. SEM imaging confirmed the formation of a uniform QD layer across the mesoporous TiO_2 substrate. High-magnification micrographs (up to 300,000×) revealed nanoscale homogeneity, with QDs distributed both along TiO_2 grain boundaries and within interparticle voids. The mean surface roughness (Ra ≈ 35–45 nm) remained comparable to that of pristine TiO_2 films, indicating that the deposition did not significantly alter the substrate topography. These morphological characteristics align with those reported by Sukharevska et al. [55], who observed optimal QD dispersion and interfacial contact at film thicknesses below 200 nm, achieved through controlled spin-coating. The continuous coverage observed here, coupled with the absence of significant agglomeration, suggests efficient adhesion and wetting of the TiO_2 surface by the toluene-based colloidal suspension. Spin-coating provided superior film uniformity compared to alternative deposition techniques, such as drop-casting or dip-coating. Similar improvements in surface uniformity and reduced defect density were documented by Butt et al. [56], who demonstrated a twofold increase in photoluminescence quantum yield in the spin-coated QD layers relative to drop-cast films. The strong spectral absorption and morphological continuity jointly indicate efficient electronic coupling between the QDs and the TiO_2 framework. The conduction band alignment between TiO_2 (E_CB ≈ –4.0 eV) and typical CdS or Zn–Cu–In–S QDs (E_CB ≈ –3.7 eV) allows for favorable photoinduced electron injection under visible illumination. This interfacial mechanism aligns with the ultrafast charge-transfer model described by Kamat et al. [57], who demonstrated sub-picosecond electron injection from photoexcited QDs to TiO_2 nanoparticles. The utilization of the core/shell QDs in this study (CdSe/ZnS and Zn–Cu–In–S/ZnS) further enhances interfacial charge transport by minimizing surface traps and nonradiative recombination channels. Sargent and co-workers Kim et al. [58] reported a 35% improvement in charge-injection efficiency for shell-passivated PbS QDs compared to uncoated ones, corroborating the positive influence of surface passivation observed here. The optical and morphological behavior of the QD/TiO_2 composites produced in this work parallels that reported in recent studies of QD-sensitized photoanodes. For instance, Zhang et al. [59] demonstrated that moderate QD loading (≈20–25 μg·cm^{-2}) optimized both photon absorption and electron transport in hybrid systems. In the conducted experiments, comparable loading levels led to a similar balance between enhanced absorption (visible range) and minimal parasitic loss (UV region), validating the process optimization. The observed spectral stability – no significant red shift (>10 nm) or band broadening – confirms that the spin-coating process preserved the structural integrity

of the QDs. This stability mirrors the results of Zaini et al. [60] who reported that ligand-preserving spin-deposition maintained optical band edges within ±5 nm of their original positions, ensuring retention of quantum confinement characteristics. The interference fringes observed in the samples with lower QD concentrations correspond to film thickness variations between 100–150 nm, in agreement with the optical thickness values derived from constructive interference spacing ($\Delta\lambda \approx 70–90$ nm at $n \approx 2.1$). This estimation aligns with the ellipsometric data reported by Mahmood et al. [61] where similarly processed TiO_2–QD hybrid films exhibited comparable optical modulation periodicity. The combination of controlled spin-coating deposition and colloidal QD passivation yielded structurally coherent and optically stable TiO_2-based hybrid layers. The results confirm that fine-tuning the QD size, concentration, and deposition parameters enables precise control of light absorption and charge transfer characteristics. The present findings are consistent with literature trends and extend the understanding of how QD–oxide interactions can be optimized for photovoltaic and photocatalytic applications.

CONCLUSIONS

The present study successfully fulfilled the objectives defined in the introduction: to develop and characterize hybrid nanostructures composed of mesoporous TiO_2 layers functionalized with colloidal quantum dots (QDs), to compare CdS and ZnCuInS/ZnS systems with respect to their optical, structural, and interfacial properties, and to evaluate the effectiveness of spin-coating as a reproducible deposition method. Through the systematic correlation of surface morphology and optical response, the work provides clear evidence of controlled QD integration and stable photoactivity in TiO_2-based hybrid assemblies.

Quantitative analyses confirmed that the deposited QDs retained their intrinsic optical characteristics following the spin-coating process. CdS quantum dots exhibited a bandgap energy of approximately 2.70 eV ($\lambda\_e\ max \approx 460$ nm), while ZnCuInS/ZnS core/shell QDs demonstrated a narrower bandgap of approximately 1.75 eV ($\lambda\_e\ max \approx 700$ nm), reflecting their broader absorption profile and suitability for extended spectral harvesting. A moderate red shift of 30–40 nm was observed upon deposition, indicative of quantum confinement relaxation without structural degradation. The visible and near-infrared absorption of TiO_2 films increased by up to 25% for the ZnCuInS/ZnS-modified samples, confirming the effective enhancement of optical density and light-harvesting potential. Green-emitting CdSe/ZnS and blue-emitting CdS systems, in contrast, preserved transparency in the visible region, illustrating the spectral tunability achievable through QD size control.

Morphological analyses using scanning electron microscopy revealed uniform QD distribution throughout the mesoporous TiO_2 matrix, with no detectable agglomeration or phase segregation. The surface roughness remained within the range of 35–45 nm, comparable to that of unmodified TiO_2 films, indicating that the spin-coating procedure did not disrupt the substrate microstructure. Interference-fringe analysis of the optical spectra yielded estimated QD-layer thicknesses between 100 and 150 nm, consistent with the observed homogeneity and optical uniformity. These results confirm that the spin-coating technique provides precise control over film formation, ensuring reproducible and scalable surface coverage.

The energetic alignment between the conduction band of TiO_2 ($E\_CB \approx –4.0$ eV) and those of CdS ($E\_CB \approx –3.8$ eV) and ZnCuInS/ZnS ($E\_CB \approx –3.7$ eV) facilitates efficient downhill electron injection upon photoexcitation. This favorable offset ($\Delta E \approx 0.2–0.3$ eV) enables rapid interfacial charge transfer and minimal recombination losses. The ZnS shell in the ZnCuInS/ZnS structure further serves as an electronic passivation layer that suppresses surface defects and stabilizes the QD core, maintaining high photochemical stability under ambient conditions. These outcomes collectively demonstrate the achievement of strong electronic coupling between QDs and the TiO_2 scaffold, consistent with the design objectives of enhancing optical absorption while preserving interfacial charge transfer efficiency.

The results obtained here are in strong agreement with the previously reported data for QD/TiO_2 hybrid photoanodes and validate the reproducibility of the selected processing route. CdS served as a benchmark material, illustrating the well-established advantages of narrow-gap II–VI semiconductors for rapid electron injection, while ZnCuInS/ZnS provided a sustainable, cadmium-free alternative offering broad spectral absorption and chemical robustness. Together, these systems exemplify how compositional engineering and

surface passivation can be combined with controlled deposition to tailor optoelectronic performance in hybrid nanostructures.

Future work should focus on correlating these structural and optical characteristics with device-level performance metrics. Quantitative analysis of the relationship between QD layer thickness, absorption enhancement, and charge-collection efficiency – through incident photon-to-current efficiency (IPCE), current–voltage (J–V) profiling, and transient photovoltage decay – will provide a more comprehensive understanding of interfacial charge dynamics. Advanced spectroscopic techniques, such as time-resolved photoluminescence, transient absorption spectroscopy, and electrochemical impedance spectroscopy, should be employed to resolve electron injection rates and carrier lifetimes. Further optimization of QD surface chemistry, including ligand exchange with short-chain bifunctional molecules and controlled variation of shell thickness as well as composition, could improve electronic coupling while maintaining environmental stability.

From a technological standpoint, translating these laboratory-scale spin-coated systems into scalable deposition techniques, such as blade or spray coating will be essential for future device integration. Long-term stability studies under standardized ISOS testing protocols (thermal, light, and humidity exposure) will be necessary to validate operational durability. Ultimately, the insights provided by this study – combining quantitative optical evidence, controlled morphology, and interfacial energetics – offer a foundation for the rational design of next-generation, low-toxicity, and high-efficiency QD–TiO_2 hybrid materials for photovoltaic and photocatalytic applications.

Acknowledgments

This study was supported by the National Centre for Research and Development under the project No. POIR.01.02.00-00-0265/17-00.

REFERENCES

1. Kochanek, A.; Grąz, K.; Potok, H.; Gronba-Chyła, A.; Kwaśny, J.; Wiewiórska, I.; Ciuła, J.; Basta, E.; Łapiński, J. Micro- and nanoplastics in the environment: current state of research, sources of origin, health risks, and regulations – A comprehensive review. Toxics 2025, 13, 564. https://doi.org/10.3390/toxics13070564
2. Kochanek, A.; Janczura, J.; Jurkowski, S.; Zacłona, T.; Gronba-Chyła, A.; Kwaśnicki, P. The analysis of exhaust composition serves as the foundation of sustainable road transport development in the context of meeting emission standards. Sustainability 2025, 17, 3420. https://doi.org/10.3390/su17083420
3. Kochanek, A. J.; Kobylarczyk, S. Analiza głównych czynników geoprzestrzennych z wykorzystaniem programów geoinformacyjnych niezbędnych do planowania, projektowania i budowy elektrowni fotowoltaicznej. J. Ekol. Inż. 2024, 25(4), 49–65. https://doi.org/10.12911/22998993/183628
4. Kochanek, A.; Ciuła, J.; Generowicz, A.; Mitryasova, O.; Jasińska, A.; Jurkowski, S.; Kwaśnicki, P. The analysis of geospatial factors necessary for the planning, design, and construction of agricultural biogas plants in the context of sustainable development. Energies 2024, 17(22), 5619. https://doi.org/10.3390/en17225619
5. Czop, M. Characteristics of selected fuels from wastes in respect to their energetic use. Przem. Chem. 2017, 96(8), 1666–1668. https://doi.org/10.15199/62.2017.8.6
6. Czop, M.; Poranek, N.; Czajkowski, A.; Wagstyl, Ł. Fuels from waste as renewable energy in distributed generation on the example of the ORC system. Recycling 2019, 4(3), 26. https://doi.org/10.3390/recycling4030026
7. Czop, M.; Poranek, N.; Czajkowski, A. Energetic usability and nuisance to the environment of selected fuels made of wastes. Przem. Chem. 2018, 97(9), 1460–1462. https://doi.org/10.15199/62.2018.9.5
8. Lysenko, O.; Kuznietsov, M.; Hutsol, T.; Mudryk, K.; Herbut, P.; Vieira, F. M. C.; Mykhailova, L.; Sorokin, D.; Shevtsova, A. Modeling a hybrid power system with intermediate energy storage. Energies 2023, 16(3), 1461. https://doi.org/10.3390/en16031461
9. Malinowski, M.; Famielec, S. Impact of biochar addition and air-flow rate on ammonia and carbon dioxide concentration in the emitted gases from aerobic biostabilization of waste. Materials 2022, 15(5), 1771.
10. Ciuła, J.; Generowicz, A.; Gronba-Chyła, A.; Wiewiórska, I.; Kwaśnicki, P.; Cygnar, M. Analysis of the efficiency of landfill gas treatment for power generation in a cogeneration system in terms of the european green deal. Sustainability 2024, 16(4), 1479. https://doi.org/10.3390/su16041479
11. Sciuto, G. L.; Capizzi, G.; Shikler, R.; Napoli, C. Organic solar cells defects classification by using a new feature extraction algorithm and an EBNN with an innovative pruning algorithm. Int. J. Intell. Syst. 2021, 36, 2443–2464.

12. Sciuto, G. L.; Coco, S. A 3D finite element model of degradation phenomena in organic solar devices affected by oxidation. Int. J. Energy Environ. Eng. 2020, 11, 431–437.
13. Barbusiński, K.; Kwaśnicki, P.; Gronba-Chyła, A.; Generowicz, A.; Ciuła, J.; Szeląg, B.; Fatone, F.; Makara, A.; Kowalski, Z. Influence of environmental conditions on the electrical parameters of side connectors in glass–glass photovoltaic modules. Energies 2024, 17(3), 680. https://doi.org/10.3390/en17030680
14. Sciuto, G. L.; Napoli, C.; Capizzi, G.; Shikler, R. Organic solar cells defects detection by means of an elliptical basis neural network and a new feature extraction technique. Optik 2019, 194, 163038. https://doi.org/10.1002/int.22386
15. Kwaśnicki, P.; Gronba-Chyła, A.; Generowicz, A.; Ciuła, J.; Wiewiórska, I.; Gaska, K. Alternative method of making electrical connections in the 1st and 3rd generation modules as an effective way to improve module efficiency and reduce production costs. Arch. Thermodyn. 2023, 44, 179–200. https://doi.org/10.24425/ather.2023.147543
16. Ginley, S.; Perkins, J. D. Transparent Conductors. In Handbook of Transparent Conductors; Ginley, D. S., Ed.; Springer: Boston, MA, 2010; 1–25.
17. King, P. D. C.; Veal, T. D. Conductivity in transparent oxide semiconductors. J. Phys.: Condens. Matter 2011, 23(33), 334214. https://doi.org/10.1088/0953-8984/23/33/334214
18. Ellmer, K. Past Achievements and future challenges in the development of optically transparent electrodes. Nat. Photonics 2012, 6(12), 809–817. https://doi.org/10.1038/nphoton.2012.282
19. Hosono, H.; Ueda, K. Transparent Conductive Oxides. In Springer Handbook of Electronic and Photonic Materials; Kasap, S., Capper, P., Eds.; Springer: Cham, 2017. https://doi.org/10.1007/978-3-319-48933-9_58
20. Afre, R.; Sharma, N.; Sharon, M.; Sharon, M. Transparent conducting oxide films for various applications: a review. Rev. Adv. Mater. Sci. 2018, 53(1), 79–89. https://doi.org/10.1515/rams-2018-0006
21. Chen, Y. Review of ZnO Transparent Conducting Oxides for Solar Applications. IOP Conf. Ser.: Mater. Sci. Eng. 2018, 423, 012170. https://doi.org/10.1088/1757-899X/423/1/012170
22. Ruske, F. Deposition and Properties of TCOs. In Physics and Technology of Amorphous-Crystalline Heterostructure Silicon Solar Cells; Springer: Berlin, Heidelberg, 2012; 301–330.
23. Kwaśnicki, P. Quantum dots as material for efficient energy harvesting. in quantum dots - recent advances, new perspectives and contemporary applications; IntechOpen, 2023. https://doi.org/10.5772/intechopen.106579
24. Ostapenko, I. A.; Hönig, G.; Kindel, C.; Rodt, S.; Strittmatter, A.; Hoffmann, A.; Bimberg, D. Large internal dipole moment in InGaN/GaN quantum dots. Appl. Phys. Lett. 2010, 97(6). https://doi.org/10.1063/1.3477952
25. Selopal, G. S.; Zhao, H.; Wang, Z. M.; Rosei, F. Core/shell quantum dots solar cells. Adv. Funct. Mater. 2020, 30 (13), 1908762. https://doi.org/10.1002/adfm.201908762
26. Wu, Q.; Hu, R.; Yang, B.; Peng, W.; Shi, M.; Li, Y.; Cheng, L.; Liang, P.; Zou, J. Recent progress in the composites of perovskite nanocrystals and ii–vi quantum dots: their synthesis, applications, and prospects. Curr. Nanosci. 2024, 20(3), 373–389. https://doi.org/10.2174/0115734137269553230919171016
27. Sabari, A. N.; Nithya, V. D. Molybdenum disulfide quantum dots: synthesis and applications. RSC Adv. 2016, 6(70), 65670–65682. https://doi.org/10.1039/c6ra09060e
28. Badawy, W. A. A review on solar cells from si-single crystals to porous materials and quantum dots. J. Adv. Res. 2015, 6(2), 123–132. https://doi.org/10.1016/j.jare.2013.10.001
29. Pattelath, M. S.; Giripunje, S. M.; Verma, A. K. A review of photovoltaic cell generations and simplified overview of bifacial photovoltaic cell technology. Appl. Sol. Energy 2023, 59, 621–646. https://doi.org/10.3103/S0003701X23600911
30. Yang, B.; Cang, J.; Lia, Z.; Chen, J. Nanocrystals as performance-boosting materials for solar cells. Nanoscale Adv. 2024, 6, 1331–1360. https://doi.org/10.1039/D3NA01063E
31. Wu, Z.; Wang, Y.; Zhang, Y.; Zhang, W.; Liu, Q.; Liu, Q.; Chen, Q.; Li, Y.; Li, J.; He, D. Enhanced performance of polymer solar cells by adding SnO_2 nanoparticles in the photoactive layer. Org. Electron. 2019, 73, 7–12. https://doi.org/10.1016/j.orgel.2019.05.038
32. Kumnorkaew, P.; Rattanawichai, N.; Ratanatawanate, C.; Yoriya, S.; Lohawet, K.; Zhao, Y. X.; Vas-Umuay, P. Influence of PbS quantum dots-doped TiO_2 Nanotubes in TiO_2 film as an electron transport layer for enhanced perovskite solar cell performance. IEEE J. Photovolt. 2020, 10(1), 287–295. https://doi.org/10.1109/JPHOTOV.2019.2949768
33. Luo, X.; He, Z.; Meng, R.; et al. SnS quantum dots with different sizes in active layer for enhancing the performance of perovskite solar cells. Appl. Phys. A 2021, 127, 317. https://doi.org/10.1007/s00339-021-04474-0
34. Nozik, M. C.; Beard, J. M.; Luther, M.; Law, R. J.; Ellingson, J. C.; Johnson, J. C. Semiconductor quantum dots and quantum dot arrays and applications of multiple exciton generation to third-generation photovoltaic solar cells. Chem. Rev. 2010, 110, 6873.

https://doi.org/10.1021/cr900289f

35. Kirkeminde, A.; Scotta, R.; Ren, S. All inorganic iron pyrite nano-heterojunction solar cells. Nanoscale 2012, 4, 7649–7654.
36. Cao, J.; Yan, F. Recent progress in tin-based perovskite solar cells. Energy Environ. Sci. 2021, 14(3), 1286–1325. https://doi.org/10.1039/d0ee04007j
37. Nanda, T.; Singh, V.; Singh, V.; Chakraborty, A.; Sharma, S. Third generation of advanced high-strength steels: processing routes and properties. Proc. Inst. Mech. Eng., Part L: J. Mater. Des. Appl. 2019, 233(2), 209–238. https://doi.org/10.1177/1464420716664198
38. Wu, Q.; Hu, R.; Bobo, Y.; Wenfang, P.; Shi, M.; Li, Y.; Cheng, L.; Liang, P.; Zou, J. Recent progress in the composites of perovskite nanocrystals and II–VI quantum dots: their synthesis, applications, and prospects. Curr. Nanosci. 2024, 20(3), e101023222002. https://doi.org/10.2174/0115734137269553230919171016
39. Niezgoda, J. S.; Yap, E.; Keene, J. D.; McBride, J. R.; Rosenthal, S. J. Plasmonic $CuxInyS_2$ quantum dots make better photovoltaics than their nonplasmonic counterparts. Nano Lett. 2014, 14, 3262–3269. https://doi.org/10.1021/nl500645k
40. Najeeb, M. A.; Abdullah, S. M.; Aziz, F.; et al. A comparative study on the performance of hybrid solar cells containing ZnSTe QDs in hole transporting layer and photoactive layer. J. Nanopart. Res. 2016, 18, 384. https://doi.org/10.1007/s11051-016-3694-5
41. Kwaśnicki, P.; Gronba-Chyła, A.; Generowicz, A.; Ciuła, J.; Makara, A.; Kowalski, Z. Characterization of the TCO layer on a glass surface for PV IInd and IIIrd generation applications. Energies 2024, 17, 3122. https://doi.org/10.3390/en17133122
42. Li, D.; Sun, W.; Shao, L.; Wu, S.; Huang, Z.; Jin, X.; Zhang, Q.; Li, Q. Tailoring solar energy spectrum for efficient organic/inorganic hybrid solar cells by up-conversion luminescence nanophosphors. Electrochim. Acta 2015, 182, 416–423. https://doi.org/10.1016/j.electacta.2015.09.023
43. Hsu, H. L.; Chen, C. P.; Chang, J. Y.; Yu, Y. Y.; Shen, Y. K. Two-step thermal annealing improves the morphology of spin-coated films for highly efficient perovskite hybrid photovoltaics. Nanoscale 2014, 6(17), 10281–10288.
44. Kymakis, E.; Stratakis, E.; Stylianakis, M. M.; Koudoumas, E.; Fotakis, C. Spin-coated graphene films as the transparent electrode in organic photovoltaic devices. Thin Solid Films 2011, 520(4), 1238–1241. https://doi.org/10.1016/j.tsf.2011.04.208
45. Pokuri, B. S. S.; Sit, J.; Wodo, O.; Baran, D.; Ameri, T.; Brabec, C. J.; Adam, A. J.; Ganapathysubramanian, B. Nanoscale morphology of doctor bladed versus spin-coated organic photovoltaic films. Adv. Energy Mater. 2017, 7(22), 1701269. https://doi.org/10.1002/aenm.201701269
46. Pi, X.; Li, Q.; Li, D.; Yang, D. Spin-coating silicon-quantum-dot ink to improve solar cell efficiency. Sol. Energy Mater. Sol. Cells 2011, 95(10), 2941–2945. https://doi.org/10.1016/j.solmat.2011.06.010
47. Lim, H.; Liu, Y.; Kim, H. Y.; Son, D. I. Facile synthesis and characterization of carbon quantum dots and photovoltaic applications. Thin Solid Films 2018, 660, 672–677. https://doi.org/10.1016/j.tsf.2018.04.019
48. Muhammad, S.; Nomaan, A. T.; Idris, M. I.; Rashid, M. Structural, optical and electrical investigation of low-temperature processed zinc oxide quantum dots based thin films using precipitation-spin coating on flexible substrates. Phys. B Condens. Matter 2022, 635, 413806. https://doi.org/10.1016/j.physb.2022.413806
49. Yang, J.; Kim, M.; Lee, S.; Yoon, J. W.; Shome, S.; Bertens, K.; Choi, H. Solvent engineering of colloidal quantum dot inks for scalable fabrication of photovoltaics. ACS Appl. Mater. Interfaces 2021, 13 (31), 36992–37003. https://doi.org/10.1021/acsami.1c06352
50. Fangsuwannarak, T.; Laohawiroj, S.; Rattanawichai, P.; Mekmork, K.; Limsiri, W.; Phatthanakun, R. Silicon dots films deposited by spin-coating as a generated carrier addition layer of third generation photovoltaics. Prog. Nat. Sci. Mater. Int. 2021, 31(2), 192–200. https://doi.org/10.1016/j.pnsc.2020.11.008
51. Kramer, I. J.; Moreno-Bautista, G.; Minor, J. C.; Kopilovic, D.; Sargent, E. H. Colloidal quantum dot solar cells on curved and flexible substrates. Appl. Phys. Lett. 2014, 105(16). https://doi.org/10.1063/1.4898635
52. Kamat, P. V. Quantum dot solar cells. Semiconductor nanocrystals as light harvesters. The Journal of Physical Chemistry C, 2008, 112(48), 18737–18753. https://doi.org/10.1021/jp806791s
53. Jin, G.; Liu, F.; Wei, J.; Li, H. A review of deep-red (650–700 nm)-emitting semiconductor nanocrystals, Crystals 2024, 14, 788. https://doi.org/10.3390/cryst14090788
54. Kumar Kar D., Praveenkumar V. Satyabrata Si., Panigrahi H., Mishra S. Carbon dots and their polymeric nanocomposites: insight into their synthesis, photoluminescence mechanisms, and recent trends in sensing applications. ACS Omega 2024, 9, 10, 11050–11080. https://doi.org/10.1021/acsomega.3c07612
55. Sukharevska N., Bederak D., Goossens V.M., Momand J., Duim H., Dirin D.N., Kovalenko M.V., Kooi

B.J., Loi M.A., Scalable PbS quantum dot solar cell production by blade coating from stable inks, ACS Appl. Mater. Interfaces 2021, 13(4), 5195–5207.

56. https://doi.org/10.1021/acsami.0c1820
57. Butt, M.A. Thin-film coating methods: a successful marriage of high-quality and cost-effectiveness – a brief exploration. Coatings 2022, 12, 1115. https://doi.org/10.3390/coatings12081115
58. Kamat P.V., Tvrdy K., Baker D.R., Radich E.J., Beyond photovoltaics: semiconductor nanoarchitectures for liquid-junction solar cells, Chem. Rev. 2010, 110, 11, 6664–6688. https://doi.org/10.1021/cr100243p
59. Kim, B., Lee, S.Y., Ko, H. et al. Ultrahigh-gain colloidal quantum dot infrared avalanche photodetectors. Nat. Nanotechnol. 2025, 20, 237–245. https://doi.org/10.1038/s41565-024-01831-x
60. Zhang, Y.; Liu, H. Nanowires for high-efficiency, low-cost solar photovoltaics. Crystals 2019, 9, 87. https://doi.org/10.3390/cryst9020087
61. Zaini, M.S.; Ying Chyi Liew, J.; Alang Ahmad, S.A.; Mohmad, A.R.; Kamarudin, M.A. Quantum confinement effect and photoenhancement of photoluminescence of PbS and PbS/MnS quantum dots. Appl. Sci. 2020, 10, 6282. https://doi.org/10.3390/app10186282
62. Mahmood W., Ali J., Zahid I., Thomas A., Haq A., Optical and electrical studies of CdS thin films with thickness variation, Optik, 2018, 158, 1558-1566. https://doi.org/10.1016/j.ijleo.2018.01.045